CHEMISTRY
A EUROPEAN JOURNAL

DOI: 10.1002/chem.200500948

Electrochemistry and Photophysics of Donor-Substituted Triarylboranes: Symmetry Breaking in Ground and Excited State

Rainer Stahl,[a] Christoph Lambert,*[a] Conrad Kaiser,[a] Rüdiger Wortmann†,[b] and Ruth Jakober[b]

Dedicated to Prof. Dr. Dr. h.c. mult. Siegfried Hünig on the occasion of his 85th birthday

Abstract: We synthesized a series of amino substituted triarylboranes (TABs) **1**–**3** by copper(I)-catalyzed cross-coupling reactions. The title compounds were investigated by means of cyclic voltammetry (CV) and UV-visible absorption and fluorescence spectroscopy. Electrochemical oxidation of tris(4-carbazolyl-2,6-dimethylphenyl)-borane (**3**) leads to the formation of an electroactive polymer film on the electrode surface. The charge-transfer (CT) absorption band of all three TABs shows a pronounced negative solvatochromism, while the emission is positively solvatochromic. By combining Jortner's theory, AM1 computations, and electrooptical absorption measurements (EOAM), this unexpected behavior was shown to be due to a dipole inversion upon $S_0 \rightarrow S_1$ excitation. Furthermore, polarized steady-state fluorescence spectroscopy and EOAM prove that the ground-state geometry of **3** is of lower symmetry than D_3 and that the excitation energy can be transferred from one subchromophore to another within the lifetime of the excited state. Exciton-coupling theory was used to quantitatively analyze this excitation transfer.

Keywords: boranes · charge transfer · fluorescence spectroscopy · solvatochromism · symmetry breaking · UV/Vis spectroscopy

Introduction

In this contribution we report the electrochemical behavior and the photophysical properties of a series of amino-substituted triarylboranes (TAB) **1**–**3** which might be useful electron- or hole-conducting materials. In recent years, TABs have attracted increasing interest due to their unique electrochemical and photophysical properties.[1,2] From the viewpoint of electrochemistry these compounds are quite good electron acceptors because of the vacant boron p_z orbital. Thus, TABs can easily be reduced to yield their corresponding radical anions. On the other hand this electron deficiency facilitates the attack of nucleophiles and, therefore, bulky substituents such as methyl or isopropyl groups in the *ortho* position to the boron atom are necessary in order to provide kinetic stability. Furthermore, TABs exhibit a pronounced fluorescence in the visible region, which can be tuned by additional substituents. High fluorescence quantum yields have been found for donor-substituted TABs in particular.[1] Owing to these properties the dimesitylboryl group has often been used as the acceptor moiety in π-conjugated donor–acceptor chromophores.[3–7]

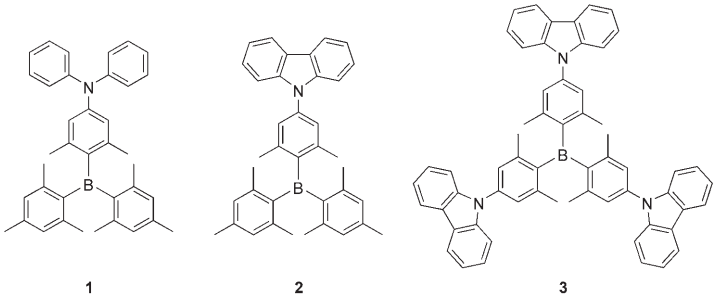

Owing to the above-mentioned features, TABs are used as emitting and/or charge-transport materials in optoelectronic devices, such as organic light-emitting diodes (OLED).[1,2,8–10] In particular the combination of TABs with

[a] Dipl.-Chem. R. Stahl, Prof. Dr. C. Lambert, C. Kaiser
Institut für Organische Chemie, Am Hubland
Julius-Maximilians-Universität Würzburg
97074 Würzburg (Germany)
Fax: (+49) 931-888-4606
E-mail: lambert@chemie.uni-wuerzburg.de

[b] Prof. Dr. R. Wortmann, Dipl.-Chem. R. Jakober
Institut für Physikalische Chemie
Technische Universität Kaiserslautern
Erwin-Schrödinger-Straße
67663 Kaiserslautern (Germany)

[†] deceased 13.03.2005

WILEY InterScience DISCOVER SOMETHING GREAT
© 2006 Wiley-VCH Verlag GmbH & Co. KGaA, Weinheim

(amino) donor moieties is a promising approach and several representatives of this type of compound have already demonstrated their suitability for use in OLEDs.[8,11–13]

To improve the performance of these materials systematically a detailed understanding of their basic electrochemical and photophysical properties is indispensable. In addition, TABs are isoelectronic to triphenylmethane cations and can therefore provide further information about this important class of dyes. Although the electrochemistry[14–16] and photophysics[17–19] of simple TABs, such as triphenylborane or trimesitylborane, have been the subject of various publications in the past decades, some aspects of the properties of their donor-substituted analogues still demand further investigation. Especially, the symmetry of the ground state, which has been studied intensively for triphenylborane and related model compounds[18,20–23] and for triphenylmethane dyes,[24,25] is still a controversial topic.

We synthesized the carbazole-substituted TAB **3**, which consists of three equivalent 1D subchromophores, and its 1D model compounds **1** and **2**. These compounds were characterized by cyclic voltammetry (CV) and UV/Vis absorption, fluorescence, and polarized steady-state fluorescence spectroscopy. Additionally, electrooptical absorption measurements (EOAM)[26] were performed.

Results and Discussion

Synthesis: The synthesis of TABs **1**–**3** is outlined in Schemes 1 and 2. The diphenylamino-substituted precursor **7** was synthesized by copper-catalyzed amination of 2-bromo-5-iodo-1,3-dimethylbenzene (**6**) with diphenylamine.[27] Lithiation of **7** and subsequent reaction of the aryllithium compound with dimesitylboron fluoride yielded the diphenylamino-substituted TAB **1**. The carbazole-substituted precursor **9** was prepared in a similar manner by copper-catalyzed amination of 2,5-dibromo-1,3-dimethylbenzene (**8**) with carbazole.[28] Conversion into the corresponding aryllithium compound and reaction with either dimesitylboron fluoride or trifluoroborane diethyletherate in the appropriate stoichiometry yielded TABs **2** and **3**, respectively.

Cyclic voltammetry (CV): The redox properties of TABs **1**–**3** were studied by CV. Due to their donor–acceptor character all compounds can be both oxidized and reduced electrochemically. The corresponding oxidation and reduction potentials are summarized in Table 1.

Table 1. Redox potentials of TABs **1**–**3** (vs Fc/Fc^+).

	1	**2**	**3**	poly-**3**[b]
E^1_{ox} [mV]	470[a,f]	860[a,d]	850[a,d,e]	620
E^2_{ox} [mV]	–	–	–	830
E_{red} [mV]	−2580[c,f]	−2480[c]	−2215[c,f]	−2190[f]

[a] 0.2 M CH_2Cl_2/TBAP. [b] 0.2 M MeCN/TBAP. [c] 0.3 M THF/TBAP. [d] Peak potential of the irreversible oxidation. [e] Shoulder at lower potential indicates multiple oxidation processes. [f] Chemically irreversible.

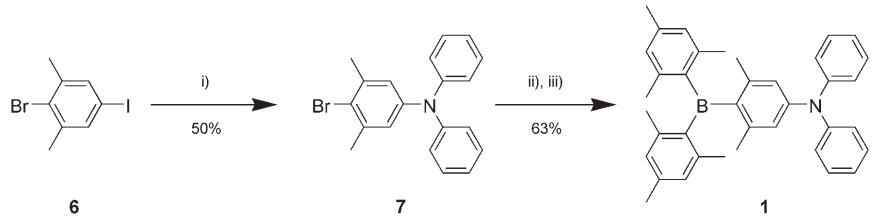

Scheme 1. Synthesis of the diphenylamino-substituted TAB **1**. i) diphenylamine, CuI, KO*t*Bu, 2,2′-bipyridine, toluene; ii) *t*BuLi, THF, −78 °C; iii) Mes_2BF, THF, −78 °C.

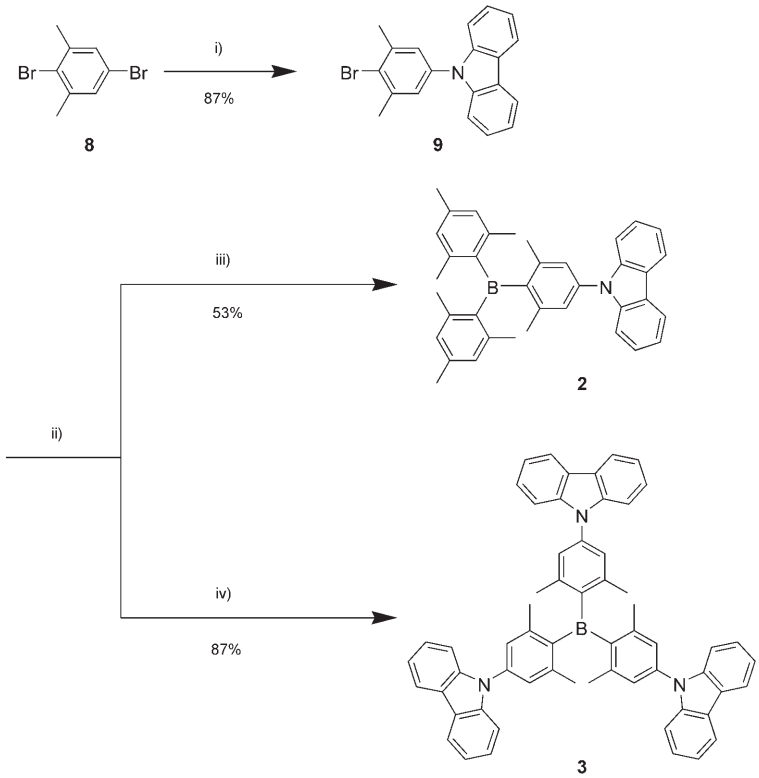

Scheme 2. Synthesis of the carbazole-substituted TABs **2** and **3**. i) carbazole, CuI, K_3PO_4, *trans*-1,2-cyclohexanediamine, 1,4-dioxane; ii) *t*BuLi, Et_2O, −78 °C; iii) Mes_2BF, Et_2O, −78 °C; iv) $BF_3{\cdot}Et_2O$, Et_2O, −78 °C.

 © 2006 Wiley-VCH Verlag GmbH & Co. KGaA, Weinheim

Both redox processes of the diphenylamino-substituted TAB **1** appear to be fully chemically reversible under semi-infinite conditions, but are in fact chemically irreversible under thin-layer conditions,[29] as the peak current decreases upon repetitive potential cycling. Moreover, a second reversible oxidation process occurs at 290 mV in a multisweep CV experiment under thin-layer conditions. This indicates the formation of dimers or oligomers of **1** through the unsubstituted *para* positions of the phenyl rings of the diphenylamino moiety. However, no indication for the formation of polymeric species was found. The reduction potential of **1** (−2.58 V vs. Fc/Fc^+ in THF) is in good agreement with that of [*p*-(dimethylamino)phenyl]dimesitylborane (**4**) (−2.16 V vs. SCE≅−2.63 V vs. Fc/Fc^+ in DMF).[16] This is surprising in so far as the π conjugation between nitrogen and boron should be more effective in **4**, because of the lack of two sterically demanding methyl groups. Therefore the electron affinity of **4** should be less than that of **1**. Evidently the N−B π–π interaction is not the crucial factor affecting the electrochemical and optical properties in this class of compounds. This is supported by the fact that the charge-transfer (CT) absorption of **4** (28200 cm^{-1} in C_6H_{12})[16,30] is significantly higher in energy than that of **1** (25300 cm^{-1} in C_6H_{12}; see below). On the other hand, the maximum CT absorption of [*p*-(diphenylamino)phenyl]-dimesitylborane (**5**) in C_6H_{12} is found at 26500 cm^{-1}.[4]

Carbazole-substituted TAB **2** is oxidized irreversibly at 860 mV under semi-infinite conditions and two new redox waves appear at 750 and 500 mV upon back reduction. This is in good agreement with the results obtained by Heinze et al. for the first oxidation cycle of *N*-phenylcarbazole.[31] Upon oxidation of the carbazole moiety the radical-cation species form dimers, which are immediately oxidized under the applied potential. In the backward scan the reduction of the dimers is observed as two new redox waves. In contrast to *N*-phenylcarbazole, which polymerizes upon multisweep oxidation in CH_3NO_2/tetrabutylammonium hexafluorophosphate (TBAHFP) to give poly-*N*-phenylcarbazole, no such polymerization was observed for compound **2** in CH_2Cl_2/tetrabutylammonium perchlorate (TBAP). This discrepancy most likely has its origin in the different solvent/electrolyte systems or in the higher monomer concentration that was used in the case of *N*-phenylcarbazole. Unfortunately, **2** is almost insoluble in CH_3NO_2 rendering it impossible to measure cyclic voltammograms in this solvent. In contrast to **1** the reduction of **2** is completely reversible even under thin-layer conditions.

TAB **3**, bearing three carbazole moieties, is also oxidized irreversibly, but upon multisweep oxidation the peak current increases with each cycle. Moreover, new redox signals appear at approximately 500 and 780 mV (see Figure 1). This clearly indicates the formation of polymers (poly-**3**) on the electrode surface with 3,3′-carbazole dimers as the bridging unit between the triarylboron centers. CV of poly-**3** was measured in a monomer-free solution of 0.2 M MeCN/TBAP (Figure 2). The fact that two discrete oxidation waves were observed at 620 and 830 mV is a further indication that no

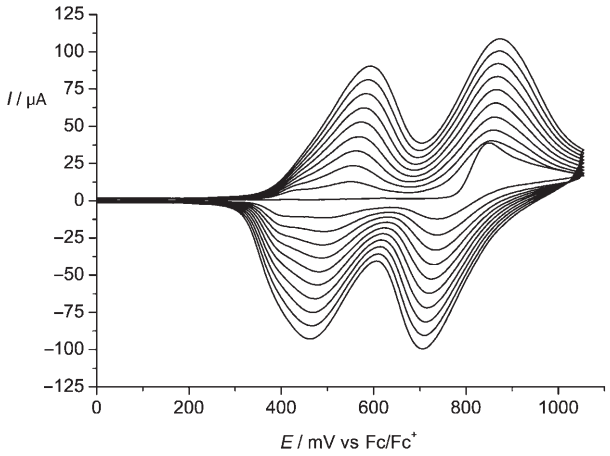

Figure 1. Multisweep CV of **3** (0.41 mM) in 0.2 M CH_2Cl_2/TBAP, $\nu = 100\ mV\,s^{-1}$, 10 cycles.

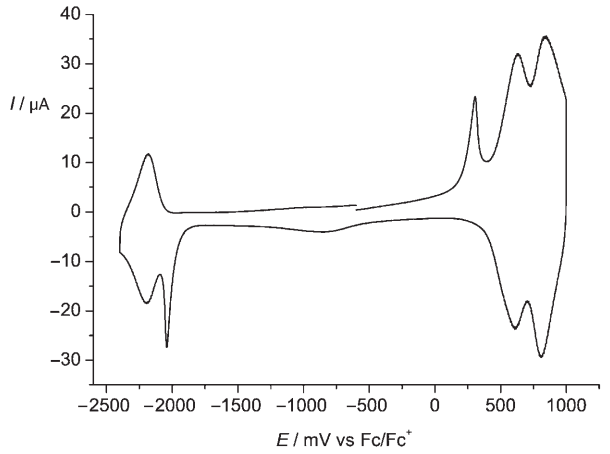

Figure 2. CV of poly-**3** in 0.2 M MeCN/TBAP, $\nu = 250\ mV\,s^{-1}$.

oligomeric carbazole chains, but only carbazole dimer units, are present in the polymer. The reduction of poly-**3** was found to be chemically irreversible as the peak current decreases with each cycle upon multisweep reduction. However, only the triarylborane part of the polymer is affected by this degeneration process as the oxidation signals of the carbazole units can still be observed, even after several reduction cycles. Another interesting feature of the redox behavior of poly-**3** is provided by the irreversible redox signals at 310 and −2040 mV. When the potential is scanned between 0 and 1000 mV several times, the oxidation signal at 310 mV disappears after the first cycle. Upon consecutive reduction a new signal is observed at −2040 mV, which again disappears after the first reduction cycle. In the following oxidation scan the signal at 310 mV is recovered. However, the origin of this "switching" behavior remains obscure.

If one compares the reduction potentials of TAB **2** and **3**, it is surprising that **3** is reduced at 270 mV less negative than **2**, although its three donor substituents should diminish the electrophilicity of the boron center. We suppose that the electron deficiency of the boron atom cannot be effectively

 © 2006 Wiley-VCH Verlag GmbH & Co. KGaA, Weinheim

stabilized by the amino donor because of the propeller-like distortion of the dimethylphenyl rings. Therefore, the inductive electron-withdrawing effect of the more electronegative nitrogen atom exceeds its mesomeric donor effect. Hence, each additional carbazole moiety increases the electrophilicity of the boron center. This indicates that the π–π interaction between B and N is rather weak in this type of chromophore; this result is also supported by the small ground-state dipole moments (see below).

Absorption and emission spectroscopy: The UV-visible absorption spectra of TABs **1**, **2**, and **3** are characterized by a low-energy CT band at 25300, 27600, and 26000 cm^{-1}, respectively, in C_6H_{12} (Figure 3).

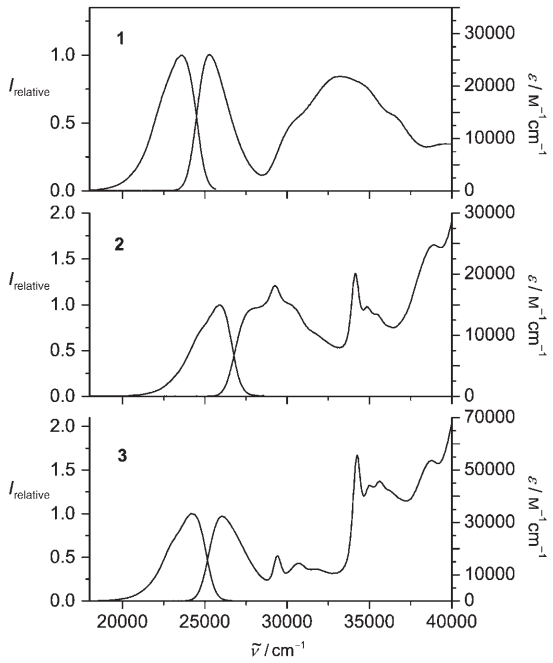

Figure 3. Absorption and emission spectra of **1**–**3** in C_6H_{12}.

The carbazole-substituted TABs **2** and **3** exhibit a very intense narrow absorption band at about 34100 cm^{-1} with a molar extinction coefficient of **3** being about three times as high as that of **2**. This band can be attributed to a local carbazole transition. Furthermore, the CT absorption band of **2** is shifted to higher wavenumbers with respect to **3**, which leads to a superposition of the CT absorption and the carbazole bands at 29400 and 30700 cm^{-1}. Similar effects have been observed recently for tricyanovinyl-substituted triarylamines and were explained in terms of electronic coupling between the subchromophores of the molecules.[32] If one presumes D_3 symmetry for **3**, the dipole–dipole interaction between the transition moments of the subchromophores of **3** leads to a splitting of the excited state into a degenerate E state and an A state, as outlined in Scheme 3.[33] This interaction is associated with an exchange of excitation energy from one subchromophore to another.[33] Provided that the

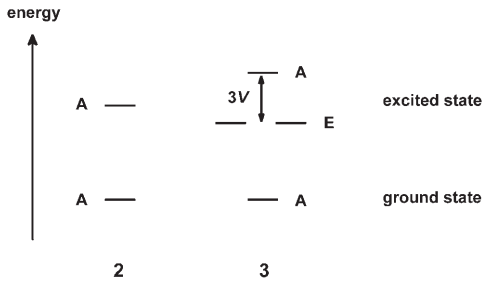

Scheme 3. Excited-state splitting of **3** with respect to **2**. The coupling integral V is a measure of the electronic interaction between the subchromophores in **3**.

orbital overlap of the three subchromophores of **3** is weak, the coupling integral V_{pq} between the transition moments of the subchromophores p and q can be approximated by the point-dipole-point-dipole model,[33] Equation (1), within the framework of the exciton coupling theory.[33–35] Parameters $\mu_{0a}^{(p)}$ and $\mu_{0a}^{(q)}$ denote the transition moments of the subchromophores p and q, respectively. The parameter R_{pq} defines the distance between the centers of the two transition moments and was calculated as the distance between the midpoints of two B–N distances (5.0 Å) of an AM1 optimized geometry of **3**; e_p, e_q, and e_{pq} denote the unit vectors of $\mu_{0a}^{(p)}$, $\mu_{0a}^{(q)}$, and R_{pq}, respectively.

$$V_{pq} = \mu_{0a}^{(p)}\mu_{0a}^{(q)}R_{pq}^{-3}\{e_p e_q - 3(e_p e_{pq})(e_q e_{pq})\} \quad (1)$$

Taking the transition moment of the model compound **2** (3.30 D) as the corresponding value for $\mu_{0a}^{(p)}$ and $\mu_{0a}^{(q)}$, a value of $V_{pq} \approx 800$ cm^{-1} (in C_6H_{12}) was calculated for **3**; this value is in qualitative agreement with the observed shift of the CT absorption band of $\Delta\tilde{\nu} = 1600$ cm^{-1} in the same solvent. It should be noted that the exciton-coupling theory can only provide a rough approximation of V, as small changes in R_{pq} have an enormous impact on the calculated value of V. Moreover, the estimation of μ_{0a} for the single chromophore **2** bears some inaccuracy, as will be discussed below.

UV/Vis absorption and fluorescence spectra of the TABs **1**, **2**, and **3** were measured in a series of solvents with different polarity ranging from C_6H_{12} to MeCN. For all compounds the emission band shows a pronounced positive solvatochromism with increasing solvent polarity (Figure 4) that is due to a large excited-state dipole moment of the fluorescent state. On the other hand, the maximum CT absorption band of all three TABs is marginally shifted to higher energies with increasing solvent polarity. Similar effects have been reported for the fluorescence of related donor-substituted tridurylboranes; however, no solvatochromism was found for the absorption of these chromophores.[36,37] It is interesting to note, that Yamaguchi et al. also observed a hypsochromic shift of approximately 1200 cm^{-1} between the amino-substituted tris(phenylethynylduryl)borane and its 1D linear analogue. This phenomenon was explained by the authors in terms of the extended π conjugation of the 2D chromophore, but may also have similar reasons (exciton coupling) as discussed above for TABs **2** and **3**.

 © 2006 Wiley-VCH Verlag GmbH & Co. KGaA, Weinheim

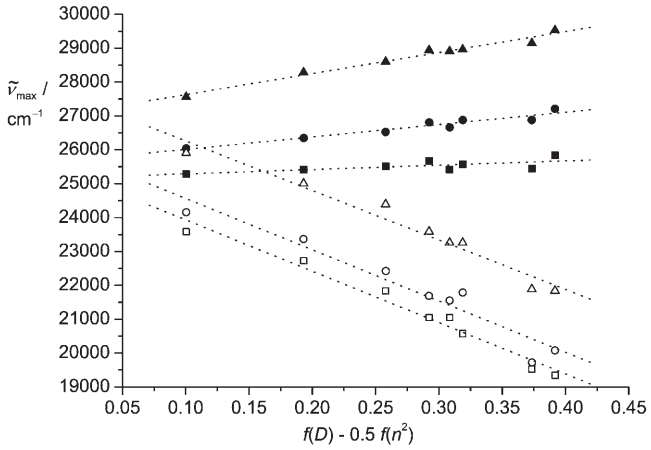

Figure 4. Absorption (filled symbols) and emission maxima (empty symbols) of **1** (squares), **2** (triangles), and **3** (circles) in solvents of different polarity (C_6H_{12}, nBu_2O, MTBE, EtOAc, THF, CH_2Cl_2, DMSO, MeCN). $f(D)-0.5f(n^2)$ is the solvent polarity function with $f(D)=(D-1)/(2D+1)$and $f(n^2)=(n^2-1)/(2n^2+1)$.

An unusual negative solvatochromic behavior, as observed for the absoption of TABs **1**–**3** has been reported before for acceptor-substituted carbazole derivatives[38,39] and may have different reasons: 1) the ground-state dipole moment $\vec{\mu}_g$ is larger than the excited-state dipole moment $\vec{\mu}_e$, 2) $\vec{\mu}_g$ and $\vec{\mu}_e$ have opposite directions, or 3) the ground-state dipole moment cannot be treated as a point dipole situated in the center of the Onsager cavity,[40] which would be a prerequisite for the validity of the Onsager–Lippert–Mataga model.[39,40] Possibility 1 would be in contrast to the solvent dependence of the emission, which suggests a large excited-state dipole moment. In the case of the C_2 symmetric molecules **1** and **2**, possibility 3 seems to be unlikely, because both $\vec{\mu}_g$ and $\vec{\mu}_e$ should be located on the long axis of symmetry between the boron and nitrogen atom, and should therefore lie in the center of the Onsager cavity. Hence, the requirements for the validity of the Onsager–Lippert–Mataga model should be fulfilled. In order to validate possibility 2 the CT absorption bands of TABs **1** and **3**[41] were analyzed by using Jortner's theory.[42–44] This model combines an average molecular vibration that is treated quantum mechanically with a classical solvent coordinate.[45] The parameters for the inner- and outer-sphere reorganization energy (λ_v and λ_o, respectively) and the parameters for the average molecular vibrational mode $\tilde{\nu}_v$ and the difference of the free energy between the diabatic ground and excited state ΔG^{00}, Equation (2), were obtained from least-squares fits of the CT absorption bands of **1** and **3** in different solvents. $S=\lambda_v/\tilde{\nu}_v$ represents the Huang–Rhys factor.

$$\varepsilon = \frac{8N\pi^3}{3000h\ln 10} n\tilde{\nu}\mu_{eg}^2 \sum_{j=0}^{\infty} \frac{e^{-S}S^j}{j!} \sqrt{\frac{1}{4\pi\lambda_0 RT}} \exp\left[-\frac{(j\tilde{\nu}_v + \lambda_0 - \tilde{\nu} + \Delta G^{00})^2}{4\pi\lambda_0 RT}\right) \quad (2)$$

A typical fit of the CT absorption band of **1** is depicted in Figure 5. In Figure 6 the resulting parameters are plotted against the solvent-polarity function given by

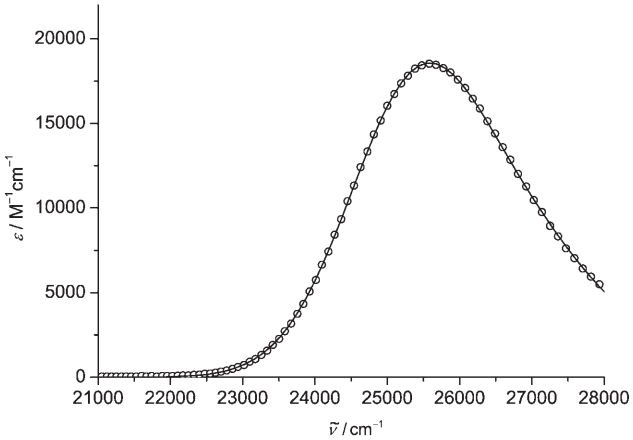

Figure 5. Typical Jortner fit (solid line) of the CT absorption band of **1** in CH_2Cl_2 (circles).

$(D\text{-}1)/(2D+1)-0.5(n^2-1)/(2n^2+1)$, in which D and n denote the permittivity and the refractive index, respectively, of the solvent. As expected from the positive solvatochromism of the emission, ΔG^{00} of **1** and **3** decreases with increasing solvent polarity due to the highly polar nature of the excited state. Concomitantly, an increase of the solvent-reorganization energy λ_o with the solvent polarity is observed. It can be rationalized from Figure 6a that in the case of **1**, ΔG^{00} is slightly overcompensated by λ_o, which gives a direct explanation for the weak hypsochromic shift of the CT absorption band described above. In the case of **3** the difference between the absolute values of the slopes of ΔG^{00} and λ_o is even higher and thus the negative solvatochromism of **3** is more pronounced (see Figure 4). The inner-sphere reorganization energy λ_v has only a weak but systematic solvent dependence for both compounds with a positive slope for **3** and a negative slope for **1** (see Figure 6c). However, the energy of the average molecular vibrational mode $\tilde{\nu}_v$ slightly increases for both **1** and **3** with increasing solvent polarity.

Additionally, the dipole moments of the ground state and the differences between the ground- and excited-state dipole moments of TABs **1**, **2**, and **3** were estimated by EOAM in 1,4-dioxane, as previously described.[26] The results are summarized in Table 2. For TABs **1** and **2** the EOAM reveal a ground-state dipole moment of $\vec{\mu}_g=0.6$ D and $\vec{\mu}_g=1.8$ D, respectively, and a dipole-moment difference of $|\Delta\vec{\mu}_{eg}|=$ 11–12 D. Comparable values for the ground-state dipole moments of both compounds **1** and **2** were obtained by AM1 calculations ($\vec{\mu}_g=0.4$ D and $\vec{\mu}_g=1.8$ D, respectively) with the dipole vector pointing from the nitrogen (negative end) to the boron (positive end). That means that upon excitation of **1** and **2** the direction of the dipole-moment vector reverses (see Scheme 4), because charge is transferred from the nitrogen to the boron center. As a consequence the solvent

 © 2006 Wiley-VCH Verlag GmbH & Co. KGaA, Weinheim

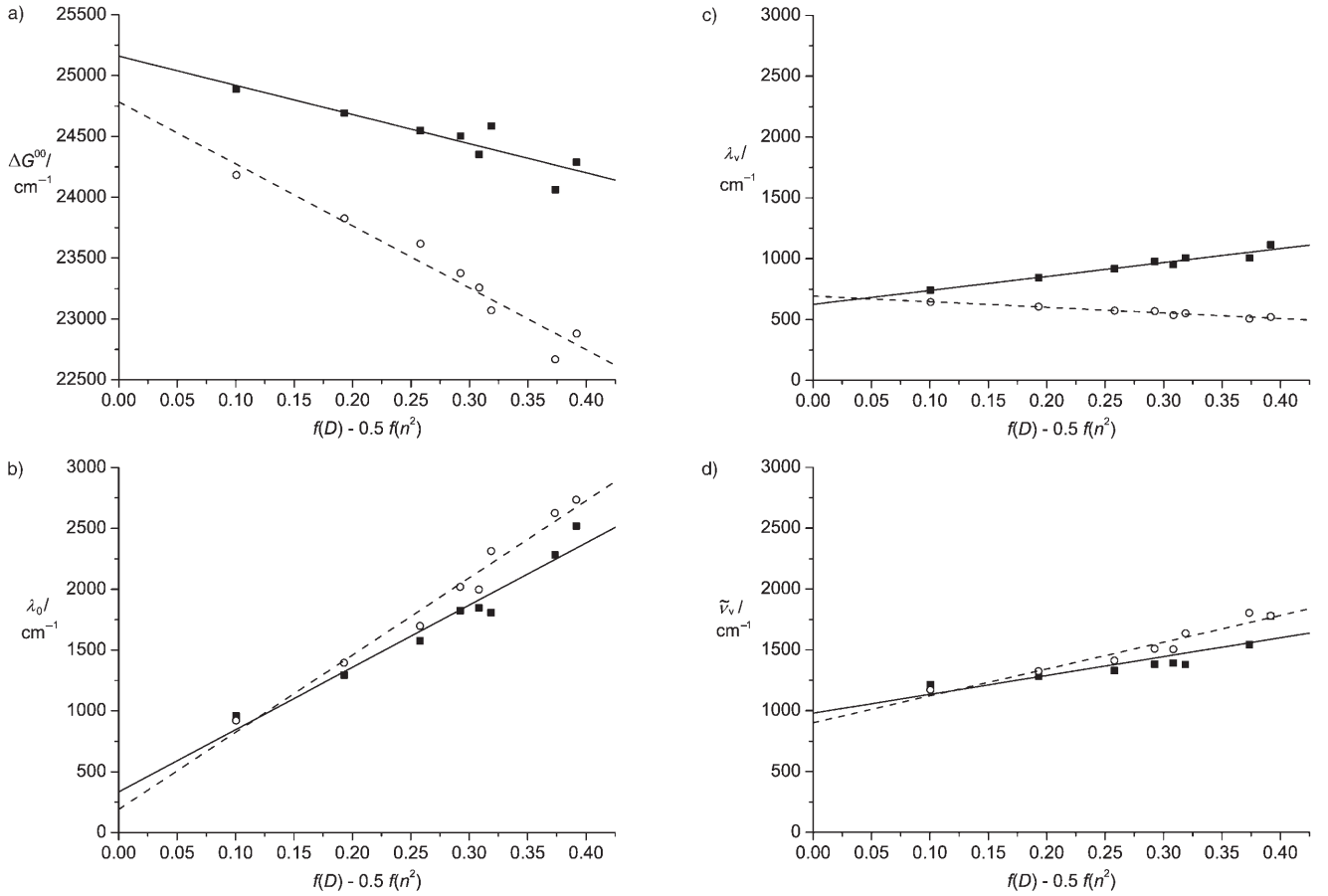

Figure 6. Plots of a) ΔG^{00}, b) λ_o, c) λ_v, and d) $\tilde{\nu}_v$ versus the solvent polarity function $f(D)-0.5f(n^2)$ for **1** (open circles) and **3** (filled squares) with $f(D)=(D-1)/(2D+1)$and $f(n^2)=(n^2-1)/(2n^2+1)$.

molecules have an energetically very unfavorable orientation after excitation into the Franck–Condon state, thus causing a distinct increase of the outer-sphere reorganization energy λ_o, especially in polar solvents. This, in turn, causes the observed negative solvatochromism, as discussed above. Relatively small ground-state dipole moments have been reported earlier by Marder and co-workers for related donor-phenyl-B(Mes)$_2$ compounds like [*p*-(dimethylamino)phenyl]-dimesitylborane (**4**) ($\vec{\mu}_g=3.0$ D).[46,47] However, positive solvatochromic behavior was observed for the CT absorption band of **4**, which implies that—in contrast to **1** and **2**—the dipole-moment vector is not reversed, but retains its original direction upon excitation of **4**. It can thus be concluded, that in the sterically less-hindered chromophore **4** the ground-state polarization is dominated by mesomeric effects, leading to a charge-separated quinoidal character with a (partially) negative boron and positive nitrogen. In **1** and **2**, because of the less-effective π conjugation, the ground-state polarization is mainly influenced by inductive effects, that is, boron is a σ donor and nitrogen is a σ acceptor. This leads to an inversed orientation of the ground-state dipoles in TABs **1** and **2** with respect to **4**.

For the 2D TAB **3**, a more sophisticated explanation of the experimental results is needed. The ground-state dipole moment of $\vec{\mu}_g=1.7$ D, estimated by EOAM suggests a lower symmetry than D_3 in the ground state (Scheme 4), in which two branches of the molecule contribute only marginally to the overall ground-state dipole moment. This unsymmetrical contribution of the three subchromophores of **3** might be caused by different torsion angles of the carbazole planes with respect to the phenyl rings, leading to a smaller ground-state polarization in two of the three branches. If one assumes that the CT excitation is mainly localized on one branch of the molecule (which is supported by the high excited-state dipole moment, see above) and that the contribution of the other two branches can be neglected, the overall excited-state dipole moment will be governed by the excited-state dipole moment of only one subchromophore. Furthermore, it seems very likely that an excitation also leads to a dipole inversion in this subchromophore, as calculated for the model compound **2**. This dipole inversion in one subchromophore will presumably cause an increase in the outer-sphere reorganization energy λ_o, which is thought to be the reason for the negative solvatochromism of the CT absorption band of the title compounds.

For comparison, the difference of the ground- and excited-state dipole moment $|\Delta\vec{\mu}_{eg}|$ was estimated according to the method of Lippert and Mataga[48–50] for all TABs **1**–**3**. Therefore, the Stokes shift between the absorption and emission maximum ($\tilde{\nu}_{abs}-\tilde{\nu}_{fl}$) in each solvent is plotted

 © 2006 Wiley-VCH Verlag GmbH & Co. KGaA, Weinheim

Table 2. Adiabatic dipole moments of the ground state and the differences between the adiabatic ground and excited state dipole moments of **1**, **2**, and **3** estimated by EOAM.

	1	**2**	**3**
$\vec{\mu}_g$/D [10^{-30} Cm]	0.57 (1.9) ± 0.15 (0.5)	1.8 (6.1) ± 0.27 (0.9)	1.7 (5.6) ± 0.06 (0.2)
$\lvert\Delta\vec{\mu}_{eg}\rvert$/D [$10^{-30}$ Cm]	11 (36) ± 0.84 (2.8)	12 (40) ± 1.1 (3.7)	11 (37) ± 0.18 (0.6)

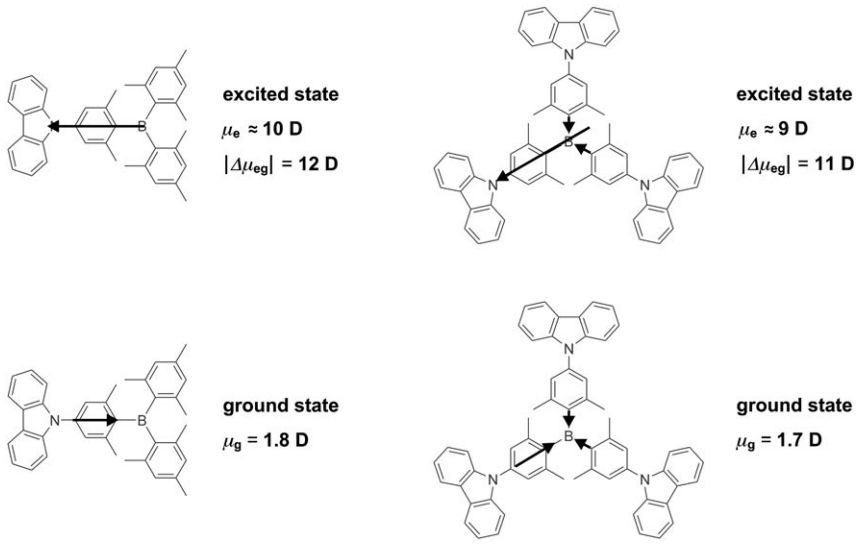

Scheme 4. Schematic representation of the ground- and excited-state dipole moments of **2** and **3**. The length of the arrows is not to scale with the absolute values of the dipole moments.

against the solvent-polarity function given by $(D-1)/(2D+1)-(n^2-1)/(2n^2+1)$ (see above). The dipole-moment difference $|\Delta\vec{\mu}_{eg}|$ can then be calculated from the slope of a linear regression of the corresponding data points using Equation (3),

$$hc(\tilde{\nu}_{abs}-\tilde{\nu}_{fl}) = hc(\tilde{\nu}^{vac}_{abs}-\tilde{\nu}^{vac}_{fl}) + \frac{2(\vec{\mu}_e-\vec{\mu}_g)^2}{a_0^3}\left[\frac{D-1}{2D+1}-\frac{n^2-1}{2n^2+1}\right] \quad (3)$$

with the solvent-dependent maxima of the CT absorption and fluorescence ($\tilde{\nu}_{abs}$ and $\tilde{\nu}_{fl}$) and the corresponding values extrapolated to the gas phase ($\tilde{\nu}^{vac}_{abs}$ and $\tilde{\nu}^{vac}_{fl}$). The effective radius of the Onsager cavity, a_0, was obtained by calculating the Connolly solvent-excluded volume from an AM1-optimized geometry of the corresponding chromophore. The radius a_0 was then calculated assuming a spherical volume for each molecule. By this method, the dipole-moment difference $|\Delta\vec{\mu}_{eg}|$ between the ground and excited states of TABs **1**–**3** was calculated to be 14, 15, and 17 D, respectively. These values are in good agreement with those estimated by EOAM taking into account that $|\Delta\vec{\mu}_{eg}| \propto a_0^3$ and therefore small changes in a_0 have an enormous impact on $|\Delta\vec{\mu}_{eg}|$. However, the estimation of a_0 is to a certain extent arbitrary.[40,48]

The transition moments of the CT absorption of TABs **1**–**3** were calculated from the integrals of the reduced absorption bands in each solvent according to Equation (4),[51] in which n is the refractive index and ε is the molar extinction coefficient.

$$\mu_{eg}^2 = \frac{3hc\varepsilon_0 \ln 10}{2000\pi^2 N}\frac{9n}{(n^2+2)^2}\int \varepsilon/\tilde{\nu}\,d\tilde{\nu} \quad (4)$$

In the case of TAB **2**—because the CT absorption band of **2** is superimposed by a local carbazole transition—the integral $\int\varepsilon/\tilde{\nu}d\tilde{\nu}$ was determined with the help of the reduced fluorescence spectrum under the assumption that the reduced absorption and fluorescence spectra exhibit a mirror-image relationship[51] (see Figure 7). It should be noted here that this method implies some inaccuracy, because the intensity of the fluorescence has to be adjusted in order to fit the CT absorption band. For comparison, the transition moments of the fluorescence were calculated from the fluorescence rate constants

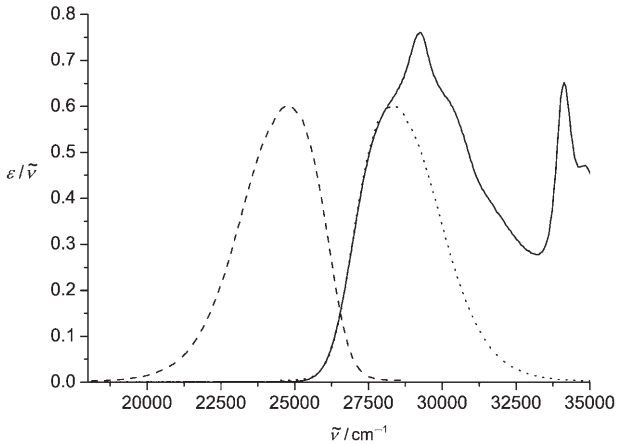

Figure 7. Reduced absorption (solid line) and fluorescence (dashed line) spectra of **2** in nBu$_2$O. The integral of the reduced absorption band $\int\varepsilon/\tilde{\nu}d\tilde{\nu}$ was calculated from the mirror image of the reduced fluorescence spectrum (dotted line).

k_f (see below) using the Strickler–Berg relationship,[52] Equation (5), in which n is the refractive index of the solvent and g_e and g_g are the degeneracy of the excited state and ground state, respectively. I_f denotes the intensity of the fluorescence against the wavenumber ($I_f = I_\lambda \times \lambda^2$). The resulting transition moments of the absorption and fluorescence are summarized in Table 3.

 © 2006 Wiley-VCH Verlag GmbH & Co. KGaA, Weinheim

Table 3. Transition moments of the CT absorption and fluorescence of TABs **1**, **2**, and **3**.

Solvent	μ_{eg}/D			μ_{fl}/D		
	1	**2**	**3**	**1**	**2**	**3**
MeCN	4.34	3.91	3.82	4.11	4.41	4.47
DMSO	3.95	4.53	4.43	4.08	4.76	4.52
CH_2Cl_2	3.99	3.82	4.72	4.10	4.62	4.54
THF	4.12	4.02	4.81	4.59	4.80	4.88
EtOAc	4.19	3.92	4.88	4.64	5.05	4.68
MTBE	4.16	3.73	4.86	4.30	5.06	5.29
nBu_2O	4.14	3.90	5.00	4.53	4.94	5.55
C_6H_{12}	4.14	3.30	4.71	4.75	5.47	5.95

$$\mu_{fl}^2 = \frac{3h\varepsilon_0}{16\times 10^6\pi^3}\frac{9}{n(n^2+2)^2}\frac{g_e}{g_g}\frac{\int \tilde{\nu}^{-3} I_f d\tilde{\nu}}{\int I_f d\tilde{\nu}} k_f \qquad (5)$$

In a molecular aggregate of N identical subchromophores, μ_{eg}^2 (which is proportional to the oscillator strength) should be N times as high as in the single chromophore, provided that the electronic interaction between the subchromophores is weak.[53] However, comparison of the μ_{eg}^2 values of **2** (as the single chromophore) and **3** (as the trimer of **2**) reveals that the μ_{eg}^2 value for **3** is only 1–2 times as high as that for **2**. This discrepancy supports the above-stated suggestion that in **3** two of the chromophore branches are twisted, which should lead to a significantly decreased absorption intensity and, consequently, lower μ_{eg}^2 values.

Differences between μ_{eg}^2 and μ_{fl}^2 of a chromophore can be regarded as an indication of a structural relaxation between the absorption and emission process. For the amino-substituted TAB **1**, μ_{fl}^2 is only somewhat higher than μ_{eg}^2, suggesting only a small structural reorganization. In the case of the carbazole-substituted TABs **2** and **3** μ_{fl}^2 is significantly higher than μ_{eg}^2, especially in solvents of low polarity. This is evidence for a distinct structural relaxation, which is thought to arise from a rotation of the carbazole moiety around the phenyl C–N bond.

The fluorescence quantum yield of compounds **1–3** was determined in a series of solvents of different polarity (see Table 4). All TABs exhibit rather high fluorescence quantum yields, as expected for this type of donor–acceptor chromophore.[1] An unexpected solvent dependence is observed especially for TAB **2**, for which ϕ_f increases significantly with increasing solvent polarity. This phenomenon can be explained by a decrease of k_{nr}, as determined from fluorescence-decay measurements (see below). However, from the solvent dependence of the fluorescence (decreasing emission energy with increasing solvent polarity) one would expect the opposite behavior, because a lowering of ΔG^{00} should cause an increase of k_{nr} (energy-gap law[54]) and consequently a decrease of ϕ_f with increasing solvent polarity.

Time-resolved fluorescence spectroscopy: The fluorescence lifetimes τ of TABs **1–3** were determined by fluorescence-decay measurements in a series of solvents with different polarity ranging from C_6H_{12} to MeCN. Additionally, the rate constants for the fluorescent and nonradiative deactivation processes, k_f and k_{nr}, were calculated according to Equations (6) and (7)

$$k_f = \frac{\phi_f}{\tau} \qquad (6)$$

$$k_{nr} = \frac{1}{\tau} - k_f \qquad (7)$$

The results are summarized in Table 4. All compounds exhibit fluorescence lifetimes in the range 2–10 ns with a pronounced solvent dependence. Surprisingly, τ increases with decreasing emission energy (increasing solvent polarity). Accordingly, opposite behavior is also found for k_{nr}, which decreases with decreasing emission energy. The origin of this unexpected behavior remains unclear. The solvent dependence of k_f (decreasing with decreasing emission energy) is in qualitative agreement with the Strickler–Berg equation (see above), which predicts a relationship of $k_f \propto \tilde{\nu}_f^3$.

Polarized steady-state fluorescence spectroscopy: Fluorescence-anisotropy measurements were performed on carbazole-substituted TABs **2** and **3** in a sucrose octaacetate (SOA) matrix at room temperature. SOA, which has a polarity similar to nBu_2O, is known to form a rigid glass after melting and cooling,[55] thus hindering rotational diffusion of the solute. This is a prerequisite to measure the limiting anisotropy r_0, which is related to the angle β between the transition moments of the absorption and emission. From Equation (8) a maximum anisotropy of 0.40 is obtained for paral-

Table 4. Fluorescence quantum yields Φ_f, fluorescence lifetimes τ, and rate constants for the fluorescent and non-radiative deactivation processes, k_f and k_{nr} of TABs **1**, **2**, and **3**.

Solvent	**1**				**2**				**3**			
	ϕ_f	$\tau/10^{-9}$ [s]	$k_f/10^8$ [s^{-1}]	$k_{nr}/10^7$ [s^{-1}]	ϕ_f	$\tau/10^{-9}$ [s]	$k_f/10^8$ [s^{-1}]	$k_{nr}/10^7$ [s^{-1}]	Φ_f	$\tau/10^{-9}$ [s]	$k_f/10^8$ [s^{-1}]	$k_{nr}/10^7$ [s^{-1}]
MeCN	0.82	10.3	0.794	1.78	0.94	7.14	1.31	0.869	0.58	11.1	0.521	3.82
DMSO	1.00	9.64	1.03	–[a]	–[b]	6.55	–[b]	–[b]	0.67	9.88	0.677	3.35
CH_2Cl_2	1.00	9.11	1.10	–[a]	0.83	4.05	2.05	4.24	0.45	5.56	0.806	9.92
THF	1.00	7.11	1.41	–[a]	0.82	3.82	2.15	4.67	0.50	5.79	0.856	8.73
EtOAc	1.00	7.44	1.34	–[a]	0.80	3.52	2.27	5.71	0.44	5.83	0.751	9.64
MTBE	0.96	7.47	1.29	0.533	0.63	2.53	2.48	14.8	0.41	3.84	1.06	15.4
nBu_2O	0.89	5.19	1.71	2.18	0.54	1.99	2.71	23.3	0.36	2.61	1.40	24.4
C_6H_{12}	0.77	3.54	2.18	6.43	0.62	1.65	3.78	22.8	0.39	2.08	1.86	29.5

[a] $k_{nr} < 10^5\ s^{-1}$. [b] Fluorescence quantum yield not measurable.

 © 2006 Wiley-VCH Verlag GmbH & Co. KGaA, Weinheim

lel orientation of the transition moments ($\beta = 0°$), whereas for perpendicular orientation ($\beta = 90°$) the minimum value is -0.20.[56]

$$r_0 = 0.4\frac{3\cos^2\beta - 1}{2} \quad (8)$$

The fluorescence-anisotropy spectra are shown in Figure 8. The emission anisotropy of the C_2 symmetric compound **2** is constant over the whole wavelength region,

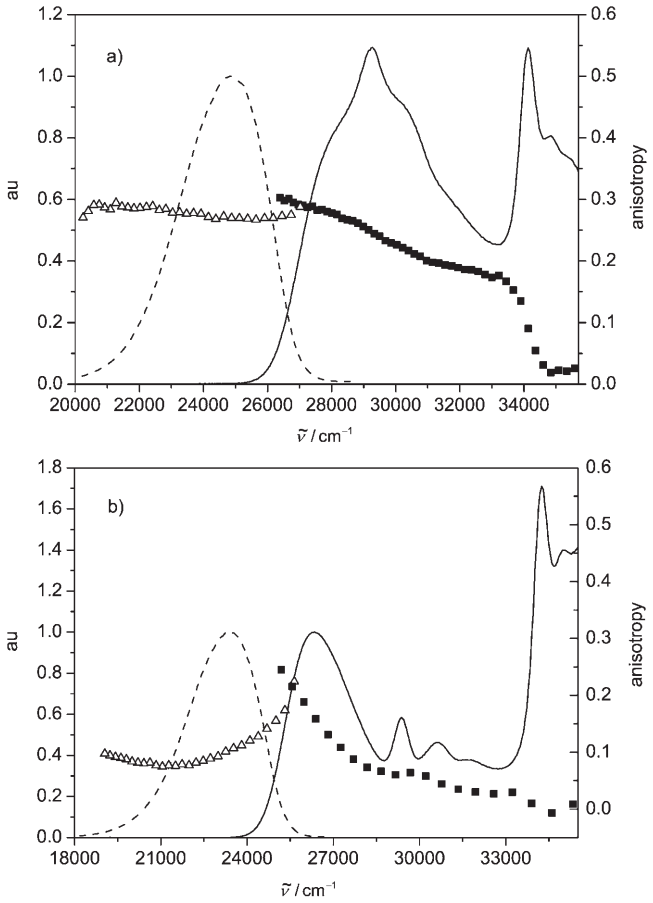

Figure 8. Anisotropy of the excitation (filled squares) and the emission (empty triangles) of a) **2** and b) **3** in a sucrose octaacetate (SOA) matrix at room temperature. The corresponding nonpolarized absorption (solid line) and emission (broken line) spectra of **2** and **3** in nBu$_2$O are added for comparison.

which means that only one transition ($S_1 \rightarrow S_0$) contributes to the emission band. The excitation anisotropy is low for the high-energy transition at 34100 cm^{-1}, indicating that the transition moments of the absorption and emission are not collinear. This is not surprising, as the absorption process at this spectral position is associated with a local carbazole transition involving a completely different transition-moment vector than for the emissive CT state. For lower excitation energies the anisotropy increases and reaches a maximum value of 0.30 at the low-energy side of the absorption spectrum ($S_0 \rightarrow S_1$ transition). At this spectral position excitation and emission involve the same electronic transition resulting in a parallel orientation of the corresponding transition moments. The fact that the excitation anisotropy does not reach the theoretical maximum value of 0.40 may indicate that there is still a small contribution from higher energy (carbazole) transitions due to the overlap of the corresponding absorption bands (see Figure 3). In case of the D_3-symmetric TAB **3** the excitation anisotropy is low (<0.1) over a wide spectral range, but increases significantly for the low-energy CT transition. This red-edge excitation effect has been observed before[57,58] and is due to an intramolecular excitation transfer between the three chromophore subunits of **3** in combination with symmetry breaking of the molecule. For molecules with a threefold symmetry (e.g., triphenylene) in which the transition moments are arranged within one plane, the additivity law of anisotropy yields a value of $r_0 = 0.1$.[59] This is because after excitation the energy can be transferred among the three branches and emission may occur from each of the three degenerate excited states with the same probability but with different transition-dipole orientations. In cases in which the symmetry of the molecule is broken and, hence, the formerly degenerate states are split, emission will preferably occur from the branch with the lowest excited-state energy (Scheme 5a)

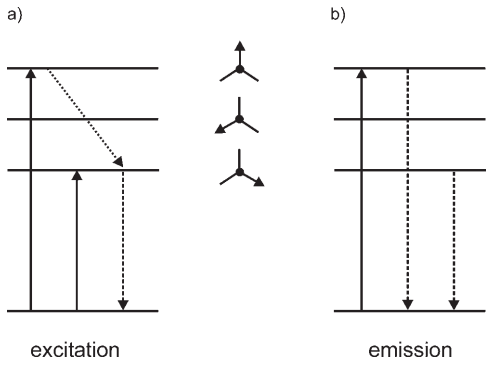

Scheme 5. Proposed electronic transitions and transition-dipole orientations of the nondegenerate excited states in **3** upon symmetry breaking. a) excitation anisotropy at a fixed emission wavelength; b) emission anisotropy at a fixed excitation wavelength.

provided that the energy transfer is fast within the excited-state lifetime. The consequence of this dipole-relaxation process is that for higher excitation energies the absorption and emission processes involve electronic transitions with different transition-dipole orientations resulting in low anisotropy. On the other hand, if excitation occurs on the low-energy side of the spectrum the energy transfer to other branches would be an uphill process. Therefore, absorption and emission involve the same transitions with identical dipole orientations resulting in an increase of the anisotropy. This phenomenon has already been observed and described in detail by De Schryver and co-workers.[58] For emission

 © 2006 Wiley-VCH Verlag GmbH & Co. KGaA, Weinheim

anisotropy an almost mirror-image behavior with respect to the excitation anisotropy is observed (Figure 8). On the low-energy side of the fluorescence spectrum the emission anisotropy is small and increases towards higher emission frequencies. This wavelength dependence also gives rise to time-dependent relaxation processes[56] and can be explained in a similar way (Scheme 5b). As excitation occurs at the high-energy side of the spectrum ($27\,000\ cm^{-1}$) it can be assumed that the energetically higher lying states are excited with a higher probability. At higher emission energies predominantly that part of the emission is observed which originates from the higher energy excited states. In this case the transition-dipole orientations of absorption and emission are parallel, resulting in a high anisotropy value. At lower energies emission of the relaxed states is detected and hence absorption and emission involve different transition-dipole orientations. Therefore, the anisotropy decreases. In agreement with the estimated ground-state dipole moment of **3** the anisotropy measurements also show that **3** adopts an asymmetric structure in SOA in the ground state.

It should be noted that for excitation anisotropy of triphenylene contrary results have been reported in literature. Leroy and Lami observed an increase of anisotropy upon red-edge excitation of triphenylene in glycerol at 203 K.[60] This phenomenon has been explained in terms of intramolecular excitation transfer in combination with symmetry breaking of the molecule. However, Hall, Valeur, and Weber were unable to reproduce these results.[59] They observed a constant value of excitation polarization of $p_0 = 0.136$ (similar to $r_0 = 0.095$) in a propylene–glycol matrix at $-70\,°C$ without any red-edge excitation effect. To check the validity of the interpretation of our experimental results, we also determined the anisotropy of triphenylene in a SOA matrix at room temperature. We tried to stick as close as possible to the procedures described by Hall, Valeur, and Weber; in particular the purification of triphenylene was carried out accurately. Surprisingly, we observed the same effect as Leroy and Lami. This leads us to the assumption that the glass matrix plays a critical role in these experiments, as it may have a great impact on the symmetry of the solute.

Conclusion

We have demonstrated that carbazole-substituted TAB **3** can be polymerized by potentiodynamic electropolymerization to form an electroactive film on the electrode surface. The resulting polymer can be switched electrochemically between a neutral, oxidized, and reduced form by applying the appropriate potential. The p-doping process is completely reversible, whereas the polymer shows only minor stability upon n-doping. In contrast to TAB **3**, the linear TABs **1** and **2** only tend to form dimers upon electrochemical oxidation. Thus, it can be concluded that in poly-**3** the TAB moieties are linked by carabzole-dimer units and no oligomeric or polymeric carbazole chains are formed. This is supported by CV measurements that show only two discrete oxidation signals for poly-**3**. Dimerization of the carbazole units instead of polymerization has also been observed recently for the chemical oxidative polymerization of 1,8-bis(*N*-carbazolyl)octane.[61]

The B–N π–π interaction in compounds **1**–**3** is rather weak, as demonstrated by CV, EOAM, and AM1 computations. Thus, the ground state of these molecules can be described by a benzoid rather than a quinoid structure. Moreover, the small ground-state polarization leads to an "inverse" ground-state dipole moment with a partial negatively charged nitrogen atom and a positively charged boron atom. Because the $S_0 \rightarrow S_1$ transition involves a CT from the nitrogen atom to the boron atom the dipole-moment vector is inverted upon CT excitation. We have successfully applied Jortner's theory to show that this dipole inversion causes a significant increase in the reorganization energy of the surrounding solvent molecules leading to the observed negative solvatochromism of the CT absorption bands of TABs **1**–**3**.

Since triphenylborane and related TABs have been shown to adopt a propeller-shaped ground-state geometry with threefold symmetry,[20–23] we initially expected TAB **3** also to possess a similar ground-state structure with D_3 symmetry. On the other hand, it has been demonstrated recently that the ground-state symmetry of various triphenylmethane dyes, like parafuchsin or crystal violet, is lowered by an interaction of one amino group with the solvent or counterion.[24] We showed by EOAM and polarized steady-state fluorescence spectroscopy that the ground state of **3** in solution is symmetry broken although the dimethylphenyl rings most likely surround the boron atom in a propeller-like fashion with local D_3 symmetry. We hypothesize that the lowering of the ground-state symmetry is due to the rotation of two carbazole moieties around the C–N bond; this hypothesis is supported by the relatively low μ_{eg}^2 values of **3** relative to **2**. Although the existence of two rotational isomers (a symmetrical and an unsymmetrical propeller form) has been suggested for tris(*p*-dimethylaminophenyl)borane,[18] this explanation is rather unlikely for **3** because of the steric congestion around the boron atom. From the solvatochromic shift of the emission of **3**, we conclude that the degeneracy of the excited *E* state (for a hypothetic D_3 symmetry) is released by Jahn–Teller distortion.

We have also demonstrated by fluorescence-anisotropy measurements that excitation energy can be transferred amongst the three subchromophores of **3**. This energy transfer can be rationalized in terms of transition dipole–dipole interactions between the chromophore subunits. We have shown how exciton-coupling theory can serve to qualitatively and quantitatively analyze the extent of the subchromophore interaction.

In conclusion we have shown that symmetry breaking may have a profound influence on the spectral properties of supposedly symmetric chromophores. These effects might be even stronger in a solid-state environment, such as that found in OLEDs.

 © 2006 Wiley-VCH Verlag GmbH & Co. KGaA, Weinheim

Experimental Section

Synthesis: All reagents were of standard quality and used as received without further purification. Boron trifluoride diethyl etherate was distilled under an inert-gas atmosphere prior to use. Reactions under inert-gas conditions (nitrogen, dried with Sicapent from Merck, traces of oxygen removed with copper oxide catalyst R3–11 from BASF) were carried out in flame-dried Schlenk vessels. The solvents were purified and dried by standard procedures and kept under an inert-gas atmosphere. Flash-column chromatography was carried out on silica gel (32–63 μm) from MP Biomedicals. The precursors **6** and **8** were prepared by a Sandmeyer-like substitutive deamination of the corresponding anilines with $CuBr_2$ according to a literature procedure.[62] Melting points were determined by using a Tottoli melting point apparatus (Büchi) and are uncorrected. ^{1}H and ^{13}C NMR spectra were recorded on a Bruker Avance 400 FT spectrometer. Electron-impact mass spectra were recorded on a Finnigan MAT 90 mass spectrometer.

(4-Bromo-3,5-dimethylphenyl)diphenylamine (7): Under a nitrogen atmosphere compound **6** (1.24 g, 4.00 mmol), diphenylamine (0.676 g, 4.00 mmol), potassium *tert*-butanolate (0.449 g, 4.00 mmol), 2,2′-bipyridine (25.0 mg, 0.160 mmol), and copper(I) iodide (30.5 mg, 0.160 mmol) were suspended in absolute toluene (3 mL) and stirred at 120 °C for 16 h. The reaction mixture was suspended in CH_2Cl_2 and washed with water. The aqueous phase was extracted with CH_2Cl_2 and the combined organic extracts were dried over $MgSO_4$. The solvent was removed in vacuo and the crude product was purified by flash chromatography with methylene chloride/petrol ether (1:9) to give **7** (0.701 g, 50 %) as a colourless solid. M.p. 168–170 °C; ^{1}H NMR (400 MHz, [D$_6$]acetone, 25 °C, TMS): $\delta = 7.29$ (m, 4H; H8), 7.07–7.02 (6H; H7, H9), 6.83 (m, 2H; H3), 2.29 ppm (m, 6H; H5); ^{13}C NMR (100 MHz, [D$_6$]acetone, 25 °C, TMS): $\delta = 148.5$, 147.7, 139.8, 130.3, 125.2, 125.1, 124.6, 124.0, 23.9 ppm; HRMS (70 eV, EI): *m*/*z* cacld for $C_{20}H_{18}BrN$: 351.06171; found: 351.06158 ($\Delta = 0.37$ ppm).

3,5-Dimethyl-4-[bis(2,4,6-trimethylphenyl)boryl]-*N*,*N*-diphenylbenzenamine (1): Under a nitrogen atmosphere *tert*-butyllithium (2.20 mL, 3.30 mmol, 1.5 M in *n*-pentane) was added dropwise to a stirred solution of **7** (0.528 g, 1.50 mmol) in absolute THF (15 mL) at −78 °C. The reaction mixture was stirred for 1 h at −78 °C and then a solution of dimesitylboron fluoride (0.483 g, 1.80 mmol) in THF (10 mL, cooled to −78 °C) was added. After stirring for 16 h at room temperature the reaction mixture was quenched with H_2O (50 mL) and extracted three times with CH_2Cl_2 (50 mL). The combined organic extracts were dried over $MgSO_4$ and the solvent was removed in vacuo. The crude product was purified by flash chromatography with methylene chloride/petrol ether (1:9→100 % CH_2Cl_2) to yield **1** (0.495 g, 63 %) as a yellow solid. M.p. 227 °C; ^{1}H NMR (400 MHz, [D$_6$]acetone, 25 °C, TMS): $\delta = 7.30$ (m, 4H; H8), 7.10–7.04 (6H; H7, H9), 6.80 (m, 2H; H12 or H12′), 6.77 (m, 2H; H12′ or H12), 6.61 (m, 2H; H3), 2.25 (m, 6H; CH_3), 2.09 (m, 6H; CH_3), 1.98 (m, 6H; CH_3), 1.90 ppm (m, 6H; CH_3); ^{13}C NMR (100 MHz, [D$_6$]acetone, 25 °C, TMS): $\delta = 149.9$, 148.4, 143.1, 141.1, 140.0, 130.3, 129.5, 125.7, 124.2, 122.5, 23.4, 23.2, 23.0, 21.3 ppm;[63] HRMS (70 eV, EI): *m*/*z* cacld for $C_{38}H_{40}{}^{10}BN$: 520.32846; found: 520.32848 ($\Delta = 0.04$ ppm).

9-(4-Bromo-3,5-dimethylphenyl)-9H-carbazole (9): Under a nitrogen atmosphere **8** (8.70 g, 33.0 mmol), carbazole (8.27 g, 49.5 mmol), copper(I) iodide (0.314 g, 1.65 mmol), *trans*-1,2-cyclohexanediamine (0.40 mL, 3.33 mmol), and potassium phosphate (22.1 g, 104 mmol) were suspended in absolute 1,4-dioxane (35 mL) and stirred for 24 h at 110 °C. The reaction mixture was suspended in CH_2Cl_2 (200 mL) and washed with water (400 mL) in small portions. The aqueous phase was extracted two times with CH_2Cl_2 (100 mL) and the combined organic extracts were dried over $MgSO_4$. The crude product was purified by flash chromatography with methylene chloride/petrol ether (1:10) to give **9** (10.0 g, 87 %) as a light-pink solid. M.p. 126 °C; ^{1}H NMR (400 MHz, [D$_6$]acetone, 25 °C, TMS): $\delta = 8.20$ (m, 2H; H9), 7.43–7.41 (6H; H3, H6, H7 or H8), 7.28 (m, 2H; H8 or H7), 2.54 ppm (m, 6H; H11); ^{13}C NMR (100 MHz, [D$_6$]acetone, 25 °C, TMS): $\delta = 141.6$, 141.1, 137.2, 127.5, 127.0, 126.6, 124.3, 121.1, 121.0, 110.7, 24.0 ppm; HRMS (70 eV, EI): *m*/*z* cacld for $C_{20}H_{16}BrN$: 349.04606; found: 349.04615 ($\Delta = 0.26$ ppm).

9-{4-[Bis(2,4,6-trimethylphenyl)boryl]-3,5-dimethylphenyl}-9H-carbazole (2): Under a nitrogen atmosphere compound **9** (0.337 g, 0.962 mmol) was dissolved in absolute diethyl ether (10 mL) and cooled to −78 °C. A solution of *tert*-butyllithium (1.28 mL, 1.92 mmol, 1.5 M in *n*-pentane) was slowly added and the yellow reaction mixture was stirred at −78 °C for 20 min. The acetone/dry-ice bath was removed and the solution was allowed to warm up. After 20 min the reaction mixture was added through a cannula to a solution of dimesitylboron fluoride (0.261 g, 0.972 mM) in diethyl ether (5 mL) that was cooled to −78 °C. The resulting suspension was stirred at −78 °C for 5 min and then at room temperature for 2 h. The reaction mixture was suspended in CH_2Cl_2 and filtered through silica gel. The solvent was removed in vacuo and the crude product was purified by flash chromatography with methylene chloride/petrol ether (1:5) to give **2** (0.270 g, 53 %) as a colorless solid. M.p. 293 °C; ^{1}H NMR (400 MHz, CD_2Cl_2, 25 °C, TMS): $\delta = 8.14$ (m, 2H; H9), 7.46 (m, 2H; H6), 7.41 (m, 2H; H7), 7.27 (m, 2H; H8), 7.14 (m, 2H; H3), 6.83 (m, 2H; H14 or H14′), 6.81 (m, 2H; H14′ or H14), 2.30 (m, 6H; CH_3), 2.11 (m, 12H; CH_3), 2.04 ppm (m, 6H; CH_3); ^{13}C NMR (100 MHz, CD_2Cl_2, 25 °C, TMS): $\delta = 142.8$, 141.2, 141.1, 141.0, 140.1, 138.5, 129.13, 129.08, 126.2, 126.0, 123.7, 120.5, 120.1, 110.4, 23.05, 23.01, 21.3 ppm; HRMS (70 eV, EI): *m*/*z* cacld for $C_{38}H_{38}{}^{10}BN$: 518.31281; found: 518.31184 ($\Delta = 1.87$ ppm).

9,9′,9″-[Borylidynetris(3,5-dimethyl-1,4-phenylene)]tris-9H-carbazole (3): Under a nitrogen atmosphere compound **9** (2.56 g, 7.31 mmol) was dissolved in absolute diethyl ether (60 mL) and cooled to −78 °C. A solution of *tert*-butyllithium (9.75 mL, 14.6 mM, 1.5 M in *n*-pentane) was slowly added and the yellow reaction mixture was stirred at −78 °C for 20 min. The acetone/dry-ice bath was removed for 20 min and the solution was allowed to warm up. The reaction mixture was cooled again to −78 °C and boron trifluoride diethyl etherate (0.30 mL, 2.4 mmol) was added dropwise. After stirring at −78 °C for 1 h the solution was stirred at room temperature for 18 h. The reaction mixture was suspended in CH_2Cl_2 (300 mL) and extracted three times with H_2O (100 mL). The aqueous phases were washed three times with CH_2Cl_2 (100 mL) and the combined organic extracts were dried over $MgSO_4$. The solvent was removed in vacuo and the crude product was purified by flash chromatography with methylene chloride/petrol ether (1:3→1:1) to give **3** (1.74 g, 87 %) as a pale-yellow solid. M.p. >300 °C; ^{1}H NMR (400 MHz, CD_2Cl_2, 25 °C, TMS): $\delta = 8.17$ (m, 6H; H9), 7.55 (m, 6H; H6), 7.46 (m, 6H; H7), 7.33–7.29 (12H; H3, H8), 2.35 ppm (m, 18H; H11); ^{13}C NMR (100 MHz, $CDCl_3$, 25 °C, TMS): $\delta = 145.8$, 142.9, 140.8, 139.2, 126.3, 126.1, 123.7, 120.5, 120.1, 110.2, 23.4 ppm; HRMS (70 eV, EI): *m*/*z* cacld for $C_{60}H_{48}{}^{10}BN_3$: 820.39721, found: 820.39805 ($\Delta = 1.02$ ppm).

UV/Vis spectroscopy: UV/Vis absorption spectra were recorded on a JASCO V-570 UV/Vis/NIR spectrometer in 1 cm quartz cells. All solvents were of spectroscopic grade and used as received.

Fluorescence spectroscopy: Steady-state fluorescence spectra were recorded on a PTI (Photon Technology International) fluorescence spectrometer model QM-2000-4 with a cooled photomultiplier (R928 P) and a 75 W xenon short arc lamp (UXL-75XE, Ushio). All spectra were recorded in 1 cm quartz cells in solvents of spectroscopic grade. The solute concentration was about 10^{-6} M and traces of oxygen were removed by bubbling a stream of argon through the solutions for about 5 mins prior to each scan. The fluorescence quantum yields of compounds **1**–**3** were determined from the absorption and fluorescence spectra according to Equation (9), in which I_f, *OD*, and *n* denote the intensity of the fluorescence, the optical density of the solution at the excitation wavelength, and the refractive index of the solvent, respectively.

$$\phi_f = \phi_{f,ref} \frac{\int I_f(\tilde{\nu})}{\int I_f(\tilde{\nu})_{ref}} \frac{OD_{ref}}{OD} \frac{n^2}{n_{ref}{}^2} \quad (9)$$

A solution of Rhodamin 101 in ethanol was used as the reference, as this compound possesses a constant quantum yield of 1.0 over a wide temperature range.[64]

Time-dependent fluorescence-decay measurements were performed with a PTI TM-2/2003 fluorescence-lifetime spectrometer with a nanosecond

 © 2006 Wiley-VCH Verlag GmbH & Co. KGaA, Weinheim

flash lamp charged with H_2/N_2 (1:1). The instrument response of the nanosecond flash lamp was determined by using colloidal silica (Ludox) in de-ionized water as a scatterer. The fluorescence-decay curves were fitted with a single-exponential decay function in order to obtain the corresponding fluorescence lifetimes.

Cyclic voltammetry (CV): CV experiments were carried out under an argon atmosphere in dry and oxygen-free solvents with 0.2–0.3 M tetrabutylammonium perchlorate (TBAP) as the supporting electrolyte. The concentration of the analyte was about 0.5 mM. A conventional three-electrode setup consisting of a platinum-disc working electrode, a Ag/AgCl pseudoreference electrode, and a platinum-wire counter electrode was used. The redox potentials were referenced against the ferrocene/ferrocenium redox couple as an internal standard. CV of the polymer was performed in monomer-free electrolyte solutions (0.2 M TBAP). After potentiodynamic electropolymerization the electrochemical cell was rinsed three times with the pure solvent and the electrolyte solution was added.

Polarized steady-state fluorescence spectroscopy: Fluorescence-anisotropy measurements were carried out in a SOA matrix at room temperature. Two Glan–Thompson polarizers from Photon Technology International were used in an L-format setup. SOA was purchased from Acros Organics and recrystalized twice from ethanol. Sample preparation was done according to a procedure reported in literature.[65] The corresponding TAB and SOA were dissolved in dichloromethane (Merck, Uvasol). The solution was filtered through a glass frit in order to remove any traces of lints and dust and purged with dry and oxygen-free argon for 10 min. Dichloromethane was partially removed in vacuo until a viscous oil resulted, which was filled into a 1 cm fluorescence quartz cuvette. The cuvette was then kept in an oven at 100 °C for about 1 h and at 150 °C for 30 mins to remove the remaining dichloromethane. The concentrations of the TABs in the SOA glass matrix were about 3 μM. In the case of TAB **2** the excitation anisotropy was measured at an emission wavenumber of 25000 cm^{-1} and for determination of the emission anisotropy the solution was excited at 28500 cm^{-1}. For TAB **3** the corresponding emission and excitation wavenumbers were 23000 and 27000 cm^{-1}, respectively.

Electrooptical absorption measurements (EOAM): The EOA technique measures the influence of the square of the electric field on the molar decadic absorption coefficient. The relative change induced by the field is a function of the wavenumber and the angle between the polarization vector of the incident light and the applied field. Typically the EOA spectrum was recorded for two polarizations (0 and 90°), and multilinear regression analyses were performed in terms of the optical-absorption spectrum; the first and second derivatives yield a set of regression coefficients from which the ground-state dipole moment and the dipole difference between the ground and excited states may be calculated.[66] EOAM spectra were recorded in 1,4-dioxane at 298 K. The solvent was dried by distillation from Na under an argon atmosphere prior to use. Details of the EOAM apparatus are given elsewhere.[67] Additional optical absorption spectra were performed with a Perkin–Elmer Lambda 900 spectrometer.

[1] C. D. Entwistle, T. B. Marder, *Chem. Mater.* **2004**, *16*, 4574–4585.
[2] C. D. Entwistle, T. B. Marder, *Angew. Chem.* **2002**, *114*, 3051–3056; *Angew. Chem. Int. Ed.* **2002**, *41*, 2927–2931.
[3] Z.-q. Liu, Q. Fang, D. Wang, D.-x. Cao, G. Xue, W.-t. Yu, H. Lei, *Chem. Eur. J.* **2003**, *9*, 5074–5084.
[4] J. C. Doty, B. Babb, M. E. Glogowski, J. L. Williams, P. J. Grisdale, *J. Organomet. Chem.* **1972**, *38*, 229–236.
[5] Z. Yuan, N. J. Taylor, Y. Sun, T. B. Marder, I. D. Williams, L. T. Cheng, *J. Organomet. Chem.* **1993**, *449*, 27–37.
[6] Z. Yuan, J. C. Collings, N. J. Taylor, T. B. Marder, C. Jardin, J. F. Halet, *J. Solid State Chem.* **2000**, *154*, 5–12.
[7] M. E. Glogowski, J. L. R. Williams, *J. Organomet. Chem.* **1981**, *216*, 1–8.
[8] Y. Shirota, M. Kinoshita, T. Noda, K. Okumoto, T. Ohara, *J. Am. Chem. Soc.* **2000**, *122*, 11021–11022.
[9] T. Noda, Y. Shirota, *J. Am. Chem. Soc.* **1998**, *120*, 9714–9715.
[10] M. Kinoshita, H. Kita, Y. Shirota, *Adv. Funct. Mater.* **2002**, *12*, 780–786.
[11] H. Doi, M. Kinoshita, K. Okumoto, Y. Shirota, *Chem. Mater.* **2003**, *15*, 1080–1089.
[12] W.-L. Jia, D.-R. Bai, T. McCormick, Q.-D. Liu, M. Motala, R.-Y. Wang, C. Seward, Y. Tao, S. Wang, *Chem. Eur. J.* **2004**, *10*, 994–1006.
[13] W.-L. Jia, X. D. Feng, D.-R. Bai, Z. H. Lu, S. Wang, G. Vamvounis, *Chem. Mater.* **2005**, *17*, 164–170.
[14] T. J. DuPont, J. L. Mills, *J. Am. Chem. Soc.* **1975**, *97*, 6375–6382.
[15] J. E. Leffler, G. B. Watts, T. Tanigaki, E. Dolan, D. S. Miller, *J. Am. Chem. Soc.* **1970**, *92*, 6825–6830.
[16] W. Kaim, A. Schulz, *Chem. Ber.* **1989**, *122*, 1863–1868.
[17] B. G. Ramsey, *J. Phys. Chem.* **1966**, *70*, 611–618.
[18] D. S. Miller, J. E. Leffler, *J. Phys. Chem.* **1970**, *74*, 2571–2574.
[19] H. Slama, C. Bräuchle, J. Voitlander, *Chem. Phys. Lett.* **1983**, *102*, 307–311.
[20] H. C. Brown, S. Sujishi, *J. Am. Chem. Soc.* **1948**, *70*, 2793–2802.
[21] T. J. Weismann, J. C. Schug, *J. Chem. Phys.* **1964**, *40*, 956.
[22] J. F. Blount, P. Finocchiaro, D. Gust, K. Mislow, *J. Am. Chem. Soc.* **1973**, *95*, 7019–7029.
[23] S. Toyota, M. Asakura, M. Oki, F. Toda, *Bull. Chem. Soc. Jpn.* **2000**, *73*, 2357–2362.
[24] H. B. Lueck, J. L. McHale, W. D. Edwards, *J. Am. Chem. Soc.* **1992**, *114*, 2342–2348.
[25] L. M. Lewis, G. L. Indig, *Dyes Pigm.* **2000**, *46*, 145–154.
[26] R. Wortmann, P. Krämer, C. Glania, S. Lebus, N. Detzer, *Chem. Phys.* **1993**, *173*, 99–108.
[27] A. A. Kelkar, N. M. Patil, R. V. Chaudhari, *Tetrahedron Lett.* **2002**, *43*, 7143–7146.
[28] A. Klapars, J. C. Antilla, X. Huang, S. L. Buchwald, *J. Am. Chem. Soc.* **2001**, *123*, 7727–7729.
[29] R. Carlier, J. Simonet, *Bull. Soc. Chim. Fr.* **1988**, *5*, 831–833.
[30] M. E. Long, *J. Lumin.* **1978**, *16*, 177–189.
[31] J. Heinze, K. Hinkelmann, M. Dietrich, J. Mortensen, *Ber. Bunsen Ges.* **1985**, *89*, 1225–1229.
[32] C. Lambert, W. Gaschler, E. Schmälzlin, K. Meerholz, C. Bräuchle, *J. Chem. Soc. Perkin Trans. 2* **1999**, 577–587.
[33] M. Kasha, H. R. Rawls, M. A. El-Bayoumi, *Pure Appl. Chem.* **1965**, *11*, 371–392.
[34] E. G. McRae, M. Kasha in *Physical Processes in Radiation Biology* (Eds.: L. Augenstein, R. Mason, B. Rosenberg), Academic Press, New York, **1964**, pp. 23–42.
[35] M. S. Gudipati, *J. Phys. Chem.* **1994**, *98*, 9750–9763.
[36] S. Yamaguchi, T. Shirasaka, K. Tamao, *Org. Lett.* **2000**, *2*, 4129–4132.
[37] W.-L. Jia, D. Song, S. Wang, *J. Org. Chem.* **2003**, *68*, 701–705.
[38] G. Meshulam, G. Berkovic, Z. Kotler, A. Ben-Asuly, R. Mazor, L. Shapiro, V. Khodorkovsky, *Synth. Met.* **2000**, *115*, 219–223.
[39] A. Kapturkiewicz, J. Herbich, J. Karpiuk, J. Nowacki, *J. Phys. Chem. A* **1997**, *101*, 2332–2344.
[40] L. Onsager, *J. Am. Chem. Soc.* **1936**, *58*, 1486–1493.
[41] A similar analysis was not possible for **2** because of the overlap of the CT absorption band with local carbazole transitions.
[42] S. F. Nelsen, M. T. Ramm, J. J. Wolff, D. R. Powell, *J. Am. Chem. Soc.* **1997**, *119*, 6863–6872.
[43] J. Cortes, H. Heitele, J. Jortner, *J. Phys. Chem.* **1994**, *98*, 2527–2536.
[44] I. R. Gould, D. Noukakis, L. Gomez-Jahn, R. H. Young, J. L. Goodman, S. Farid, *Chem. Phys.* **1993**, *176*, 439–456.
[45] P. Y. Chen, T. J. Meyer, *Chem. Rev.* **1998**, *98*, 1439–1477.
[46] Z. Yuan, N. J. Taylor, T. B. Marder, I. D. Williams, S. K. Kurtz, L.-T. Cheng in *Organic Materials for Non-linear Optics II* (Eds.: R. A. Hann, D. Bloor), The Royal Society of Chemistry, Cambridge, **1991**, pp. 190–196.
[47] Z. Yuan, C. D. Entwistle, J. C. Collings, D. Albesa-Jove, A. S. Batsanov, J. A. K. Howard, H. M. Kaiser, D. E. Kaufmann, S.-Y. Poon, W.-Y. Wong, C. Jardin, S. Fathallah, A. Boucekkine, J.-F. Halet, T. B. Marder, *Chem. Eur. J.* **2006**, *12*: DOI: 10.1002/chem.200501096.
[48] E. Lippert, *Z. Naturforsch., A* **1955**, *10*, 541–545.

 © 2006 Wiley-VCH Verlag GmbH & Co. KGaA, Weinheim

[49] N. Mataga, Y. Kaifu, M. Koizumi, *Bull. Chem. Soc. Jpn.* **1955**, *28*, 690–691.
[50] J. Herbich, A. Kapturkiewicz, *J. Am. Chem. Soc.* **1998**, *120*, 1014–1029.
[51] J. B. Birks, *Photophysics of Aromatic Molecules*, Wiley, New York, **1970**.
[52] S. J. Strickler, R. A. Berg, *J. Chem. Phys.* **1962**, *37*, 814–822.
[53] S. Gnanakaran in *Resonance Energy Transfer* (Eds.: D. L. Andrews, A. A. Demidov), Wiley, New York, **1999**, pp. 323–328.
[54] R. Englman, J. Jortner, *Mol. Phys.* **1970**, *18*, 145–164.
[55] G. J. Cox, J. H. Ferguson, M. L. Dodds, *Ind. Eng. Chem.* **1933**, *25*, 968–970.
[56] J. R. Lakowicz, *Principles of Fluorescence Spectroscopy*, 2nd ed., Kluwer Academic/Plenum, New York, **1999**.
[57] A. A. Demidov, D. L. Andrews, *Photochem. Photobiol.* **1996**, *63*, 39–52.
[58] W. Verbouwe, M. van der Auweraer, F. C. De Schryver, J. J. Piet, J. M. Warman, *J. Am. Chem. Soc.* **1998**, *120*, 1319–1324.
[59] R. D. Hall, B. Valeur, G. Weber, *Chem. Phys. Lett.* **1985**, *116*, 202–205.
[60] E. Leroy, H. Lami, *Chem. Phys. Lett.* **1976**, *41*, 373–377.
[61] E. Cloutet, C. Olivero, D. Ades, M.-C. Castex, A. Siove, *Polymer* **2002**, *43*, 3489–3495.
[62] M. P. Doyle, B. Siegfried, J. F. Dellaria, Jr., *J. Org. Chem.* **1977**, *42*, 2426–2431.
[63] Interaction of the boron-bonded carbon atoms with the quadrupole moment of the boron nucleus leads to line broadening. As a consequence these carbon atoms are not observed in the ^{13}C NMR spectrum.
[64] T. Karstens, K. Kobs, *J. Phys. Chem.* **1980**, *84*, 1871–1872.
[65] R. C. Dorfman, Y. Lin, M. D. Fayer, *J. Phys. Chem.* **1989**, *93*, 6388–6396.
[66] R. Wortmann, K. Lukaszuk in *Nonlinear Optical Responses of Molecules, Solids and Liquids: Methods and Applications* (Ed.: M. G. Papadopoulus), Research Signpost, Trivandrum (India), **2003**, pp. 179–193.
[67] W. Baumann, *Ber. Bunsen-Ges.* **1976**, *80*, 231–240.

Received: August 4, 2005
Published online: December 16, 2005

 © 2006 Wiley-VCH Verlag GmbH & Co. KGaA, Weinheim